Hindawi Publishing Corporation
EURASIP Journal on Image and Video Processing
Volume 2010, Article ID 250768, 16 pages
doi:10.1155/2010/250768

Research Article

Multiplicative Noise Removal via a Novel Variational Model

Li-Li Huang,[1,2] Liang Xiao,[1] and Zhi-Hui Wei[3]

[1] *School of Computer Science and Technology, Nanjing University of Science and Technology, Nanjing 210094, China*
[2] *Department of Information and Computing Science, Guangxi University of Technology, Liuzhou 545006, China*
[3] *Department of Applied Mathematics, Nanjing University of Science and Technology, Nanjing 210094, China*

Correspondence should be addressed to Liang Xiao, xiaoliang@mail.njust.edu.cn

Received 30 March 2010; Revised 5 May 2010; Accepted 2 June 2010

Academic Editor: Lei Zhang

Multiplicative noise appears in various image processing applications, such as synthetic aperture radar, ultrasound imaging, single particle emission-computed tomography, and positron emission tomography. Hence multiplicative noise removal is of momentous significance in coherent imaging systems and various image processing applications. This paper proposes a nonconvex Bayesian type variational model for multiplicative noise removal which includes the total variation (TV) and the Weberized TV as regularizer. We study the issues of existence and uniqueness of a minimizer for this variational model. Moreover, we develop a linearized gradient method to solve the associated Euler-Lagrange equation via a fixed-point iteration. Our experimental results show that the proposed model has good performance.

1. Introduction

Image denoising is an inverse problem widely studied in signal and image processing fields. The problem includes additive noise removal and multiplicative noise removal. In many image formation model, the noise is often modeling as an additive Gaussian noise: given an original image u, it is assumed that it has been corrupted by some Gaussian additive noise v. The denoising problem is then to recover u from the data $f = u + v$. There are many effective methods to tackle this problem. Among the most famous ones are wavelets approaches [1, 2], stochastic approaches [3], principal component analysis-based approaches [4, 5], and variational approaches [6]. We refer the reader to the literature [7, 8] and references herein for an overview of the subject.

In this paper, we focus on the issue of multiplicative noise removal. Specifically, we are interested in the denoising of SAR images. According to [9] and other references, the noise in the observed SAR image is a type of multiplicative noise which is called speckle. And the image formation model is

$$f = uv, \tag{1}$$

where f is the observed image, u is the original SAR image, and v is the noise which follows a Gamma Law with mean one. Speckle is one of the most complex image noise models. It is signal independent, non-Gaussian, and spatially dependent. Hence speckle denoising is a very challenging problem compared with additive Gaussian noise.

Multiplicative noise removal methods have been discussed in many reports. Popular methods include local linear minimum mean square error approaches [10, 11], anisotropic diffusion methods [12–15], and nonlocal means (NL-means) [16], which will not be addressed in this paper. We will focus on the variational approach-based multiplicative noise removal, especially that our researches will emphasis on TV-based methods.

To the best of our knowledge, there exist several variational approaches devoted to multiplicative noise removal problem. The first total variation-based multiplicative noise removal model (RLO-model) was presented by Rudin et al. [17], which used a constrained optimization approach with two Lagrange multipliers. Multiplicative model (AA-model) with a fitting term derived from a maximum a posteriori (MAP) was introduced by Aubert and Aujol [18]. Recently, Shi and Osher [19] adopted the data term of the AA-model

but to replace the regularizer TV(u) by TV($\log u$). Moreover, setting $w = \log u$, then they derived the strictly convex TV minimization model (SO-model). Afterwards, Huang et al. [20] modified the SO-model by adding a quadratic term to get a simpler alternating minimization algorithm. Similarly with SO-model, Bioucas and Figueiredo [21] converted the multiplicative model into an additive one by taking logarithms and proposed Bayesian type variational model. Steidl and Teuber [22] introduced a variational restoration model consisting of the I-divergence as data fitting term and the total variation seminorm as regularizer. A variational model involving curvelet coefficients for cleaning multiplicative Gamma noise was considered in [23].

As information carriers, all images are eventually perceived and interpreted by the human visual system. As a result, many researchers have found that human vision psychology and psychophysics play an important role in the image processing. Among them, Shen [24] has proposed Weberized TV model to remove Gaussian additive noise which incorporated the well-known psychological results—*Weber's Law*.

However, the previous multiplicative removal models pay a little attention to this point. Inspired by the Weberized TV regularization method [24, 25], we propose a nonconvex variational model for multiplicative noise removal. Then we prove the existence and uniqueness of a minimizer for the new model. Moreover, we develop an iterative algorithm based on the linearization technique for the associated nonlinear Euler-Lagrange equation. Our experimental results show that the proposed model has good performance.

The outline of this paper is as follows. In Section 2, we derive a new nonconvex variational model to remove multiplicative Gamma noise under the MAP framework. Moreover, we carry out the mathematic analysis of the variational model in the continuous setting. In Section 3, we develop a linearized gradient method to solve the associated Euler-Lagrange equation via a fixed-point iteration and illustrate our algorithm by displaying some numerical examples. We also compare it with other ones. Finally, concluding remarks are given in Section 4.

2. The Proposed Model and Mathematical Analysis

In this section, we propose the multiplicative noise removal model from the statistical perspective using Bayesian formulation, for which we prove the existence and uniqueness of a solution.

2.1. MAP-Based Multiplicative Noise Modeling. Let $f, u, v \in \mathrm{R}_+^n$ denote n-pixels instances of some random variables F, U, and V. Adopting a conditionally independent multiplicative noise model, we have

$$F_i = U_i V_i, \quad \text{for } i = 1, \ldots, n, \tag{2}$$

where V is an image of independent and identically distributed (i.i.d) noise random variables with mean one, following Gamma density:

$$P_V(v) = \frac{L^L}{\Gamma(L)} v^{L-1} \exp(-Lv) \cdot 1\{v > 0\}. \tag{3}$$

After standard computation, we get

$$P_{F|U}(f \mid u) = \frac{L^L}{u^L \Gamma(L)} f^{L-1} \exp\left(-\frac{Lf}{u}\right). \tag{4}$$

Under the MAP frameworks, the original image is inferred by solving a minimization problem with the form

$$\min_U \{-\log P(U \mid F)\} = \min_U \{-\log P(U) - \log P(F \mid U)\}. \tag{5}$$

We assume that U follows a Gibbs prior: $p_U(u) = (1/C)\exp(-\gamma\varphi(u))$, where C is a normalizing constant, and φ a nonnegative given function. Moreover, since V is i.i.d, therefore we have $P(F \setminus U) = \prod_{i=1}^n P(F_i \setminus U_i)$. Then, the previous computation leads us to propose the following model for restoring images corrupted with Gamma noise:

$$\min_u \left\{ \int_\Omega \left(\log u + \frac{f}{u} \right) \mathrm{d}x + \frac{\gamma}{L} \int_\Omega \varphi(u) \mathrm{d}x \right\}. \tag{6}$$

Here, the first term is the image fidelity term which measures the violation of the relation between u and the observation f. The second term is the regularization term which imposes some prior constraints on the original image and to a great degree determines the quality of the recovery image. And γ is the regularization parameter which controls the tradeoff between the fidelity term and regularization term.

2.2. Our Variational Model. As stated above, the choice of $\varphi(u)$ is important. To the best knowledge of our known, total variational functional TV(u) has been brought into wide use ever since its introduction by Rudin et al. [6]. TV(u) is defined by

$$\mathrm{TV}(u) = \int_\Omega |Du| = \sup_{p \in C_0^1, \| |p| \|_\infty \le 1} \int_\Omega u \ \mathrm{div}\ p \, \mathrm{d}x, \tag{7}$$

which reads for $L^1(\Omega)$ functions with weak first derivatives in $L^1(\Omega)$ as

$$\mathrm{TV}(u) = \int_\Omega |\nabla u| \mathrm{d}x. \tag{8}$$

This definition for the TV functional does not require differentiability or even continuity of u. In fact one of the remarkable advantages of using TV functional for image restoration is to preserve edges due to its jump discontinuities.

As an image model, TV(u) does not take into account that our visual sensitivity to the regularity or local fluctuation $|\nabla u|$ depends on the ambient intensity level u [24]. Since all images are eventually perceived and interpreted by the

Human Visual System (HVS), as a result, many researchers have found that human vision psychology and psychophysics play an important role in image processing. The classical example is the using of the Just Noticeable Difference Model (JND) in image coding and watermarking techniques [26, 27]. In these fields, the JND model is used to control the visual perceptual distortion during the coding procedure and watermark embedding. Weber's law was first described in 1834 by German physiologist Weber [28]. The law reveals the universal influence of the background stimulus u on human's sensitivity to the intensity increment $|\nabla u|$, or so called JND, in the perception of both sound and light:

$$\frac{|\nabla u|}{u} = \text{const.} \tag{9}$$

According to Weber's law, when the mean intensity of the background is increasing with a higher value, then the intensity increment $|\nabla u|$ also has higher value. In literature [24], the authors proposed a nonconvex variational model for additive Gaussian noise removal:

$$\hat{u} = \arg\min_{u \in D(\Omega)} \left\{ \lambda \int_\Omega (f-u)^2 \mathrm{d}x + \int_\Omega \frac{|Du|}{u} \right\}, \tag{10}$$

where

$$\begin{aligned} D(\Omega) = \Big\{ & u > 0 : u \in L^2(\Omega), TV(\log u) \\ & = \int_\Omega |Du|/u < \infty, u \geq f/2 \Big\}. \end{aligned} \tag{11}$$

The essential idea of the above model (10) is that it replaces the TV functional by the functional $\int_\Omega \varphi(u) = \int_\Omega |Du|/u$, the well known perceptual law-Weber's law, in the classical TV image restoration model of Rudin et al. [6].

Considering that our visual sensitivity to the local fluctuation depends on the ambient intensity level u, we take the regularization term as follows:

$$J(u) := \int_\Omega \varphi(u) \mathrm{d}x = \int_\Omega \phi(u) |Du|. \tag{12}$$

According to the different purposes of image processing, we can design different $\phi(u)$. As stated previously, we adopt $\phi(u) = \alpha_1 + \alpha_2/u$ and propose the following multiplicative denoising variational model:

$$\begin{aligned} \hat{u} &= \min_u \left\{ E(u) = J(u) + \int_\Omega \left(\log u + \frac{f}{u} \right) \mathrm{d}x \right\} \\ &= \min_u \left\{ E(u) = \alpha_1 \int_\Omega |Du| \right. \\ &\quad \left. + \alpha_2 \int_\Omega \frac{|Du|}{u} + \int_\Omega \left(\log u + \frac{f}{u} \right) \mathrm{d}x \right\}, \end{aligned} \tag{13}$$

where the first two terms are the regularization terms, while the third one is the nonconvex data fidelity term following the MAP estimator for multiplicative Gamma noise. α_1, α_2 are regularization parameters, and $f > 0$ in $L^\infty(\Omega)$ is the given data. The first regularization term is the TV functional, which preserves important structures such as edges, an important visual cue in human and computer vision. The second term $E_w(u) := \mathrm{TV}(\log u) = \int_\Omega |Du|/u$ is the well-known Weberized TV regularization term. To briefly explain the role of this term, we assume that u has a gradient $\nabla u \in L^1(\Omega)^2$, then $\mathrm{TV}(\log u) = \int_\Omega |Du|/u = \int_\Omega |\nabla u|/u \, \mathrm{d}x$ and the Weberized local variation is

$$|\nabla u|_w := \frac{|\nabla u|}{u} = \frac{1}{u} \frac{\partial u}{\partial \vec{n}}, \quad \vec{n} = \frac{\nabla u}{|\nabla u|} \tag{14}$$

which encodes the influence of the background intensity according to Weber's law (9).

The formulation (13) seems to include previous models.

(i) When $\alpha_1 = 0$, this reduces to the SO-model [19] by letting $w = \log u$.

(ii) When $\alpha_2 = 0$, this reduces to the AA-model [18].

The current paper is devoted to the study of the mathematical properties of this new model, including issues related to the existence and uniqueness of the minimizer, and its computational approach.

2.3. Mathematical Properties of the Variational Model (13). In this subsection, we first give the admissible space for the restoration model (13) and then investigate the existence and uniqueness of the minimizer to the model. Throughout the paper, we assume that $\Omega \subset \mathrm{R}^2$ is a Lipschitz open domain with a finite Lebesgue measure $|\Omega| < \infty$.

Since u denotes the intensity value, thus $u \geq 0$. When $u = 0$, it is the singularity of both Weber's fraction (9) and the Weberized local variation (14). Hence, technically we should stay away from this point and assume that $u > 0$.

First, we give the admissible space for the restoration model (13). The regularization term

$$J(u) = \int_\Omega \left(\alpha_1 + \frac{\alpha_2}{u} \right) |Du| \tag{15}$$

can be understood in the sense of the following coarea formula.

Lemma 1. *(Coarea formula). Let $\phi(u) : R^+ \to R^+$ be a C^1 function and $u \in BV(\Omega)$; then*

$$\int_\Omega \phi(u) |Du| = \int_0^\infty \phi(\lambda) H(\partial\Omega_\lambda) \, d\lambda. \tag{16}$$

Here the level set is $\Omega_\lambda = \{x : u(x) < \lambda\}, H(\partial\Omega_\lambda)$ is the perimeter of the set Ω_λ, and the space $BV(\Omega)$ is of functions of bounded variation consisting of all $L^1(\Omega)$ functions with $\int_\Omega |Du| < \infty$.

Proof. Applying [26, Theorem 2.7], we get the conclusion. □

From Lemma 1, we give the following nature admissible space for the restoration model (13):

$$\Pi(\Omega) = \left\{ u \in \mathrm{BV}(\Omega) : u > 0, \mathrm{TV}(\log u) = \int_\Omega |Du|/u < \infty \right\}. \tag{17}$$

Figure 1: The original, noisy, and restored "Lena" images: (a) noiseless image; (b) noisy image with $L = 33$; denoised images by (c) RLO method; (d) AA method; (e) HMW method ($\alpha_1 = 19, \alpha_2 = 0.0049$); (f) the proposed method ($\alpha_1 = 0.001, \alpha_2 = 0.01$).

When $\phi = 1$, we note that (16) is precisely the classical coarea formula. It means that $\mathrm{TV}(u) < \infty$, when $\mathrm{TV}(\log u) < \infty$. We shall work with $\Pi(\Omega)$ from now on.

Secondly, we give a theorem on the existence and uniqueness of the solution of the problem (13), respectively.

Theorem 1 (Existence). *Suppose that $f \in L^\infty(\Omega)$ with $\inf_\Omega f > 0$; then problem (13) has at least one minimizer in the admissible space $\Pi(\Omega)$.*

Theorem 2 (Uniqueness). *Assume that $\alpha_1 > 0$, $\alpha_2 > 0$, $f > 0$ is in $L^\infty(\Omega)$, and u is a minimizer of the restoration energy $E(u)$. Then u is unique if*

$$0 < u < f + \sqrt{f^2 + kf}, \quad \text{where } k = \alpha_2/\alpha_1. \tag{18}$$

For the proof of the existence and uniqueness see the appendix for details.

3. Numerical Results

In this section, we present some numerical examples to demonstrate the performance of our method. We also compare it with some existing other ones. All experiments were performed under Windows XP and MATLAB v7.1 running on a desktop with an Intel (R) Pentium (R) Dual E2180 Processor 2.00 GHZ and 0.99 GB of memory.

3.1. Algorithm. To numerically compute a solution to the problem (13), as in [24, 29, 30], we apply the linearization technique to iteratively solve the associated Euler-Lagrange equation, which we call "lagged diffusivity fixed point iteration". Since total variation functional is nonsmooth, which caused the main numerical difficulty, we replace the total variation functional by a smooth approximation like

$$\mathrm{TV}_\varepsilon(u) = \int_\Omega \sqrt{|\nabla u|^2 + \varepsilon}\, \mathrm{d}x \tag{19}$$

in (13). Here $\varepsilon > 0$ is the regularized parameter chosen near 0.

We first give a computational lemma.

Lemma 2. *Let $\phi(u) : R^+ \to R^+$ be a C^1 function and*

$$J(u) = \int_\Omega \phi(u)\sqrt{|\nabla u|^2 + \varepsilon}\, dx. \tag{20}$$

Then the formal Euler-Lagrange differential of $J(u)$ is

$$\frac{\partial J}{\partial u} = -\phi(u)\,\mathrm{div}\left(\frac{\nabla u}{\sqrt{|\nabla u|^2 + \varepsilon}}\right)\Bigg|_\Omega + \frac{\phi(u)}{\sqrt{|\nabla u|^2 + \varepsilon}}\frac{\partial u}{\partial \vec{n}}\Bigg|_{\partial\Omega}. \tag{21}$$

Proof. Applying Green's identity, we directly compute the first Gateaux derivative of $J(u)$ and get the conclusion. □

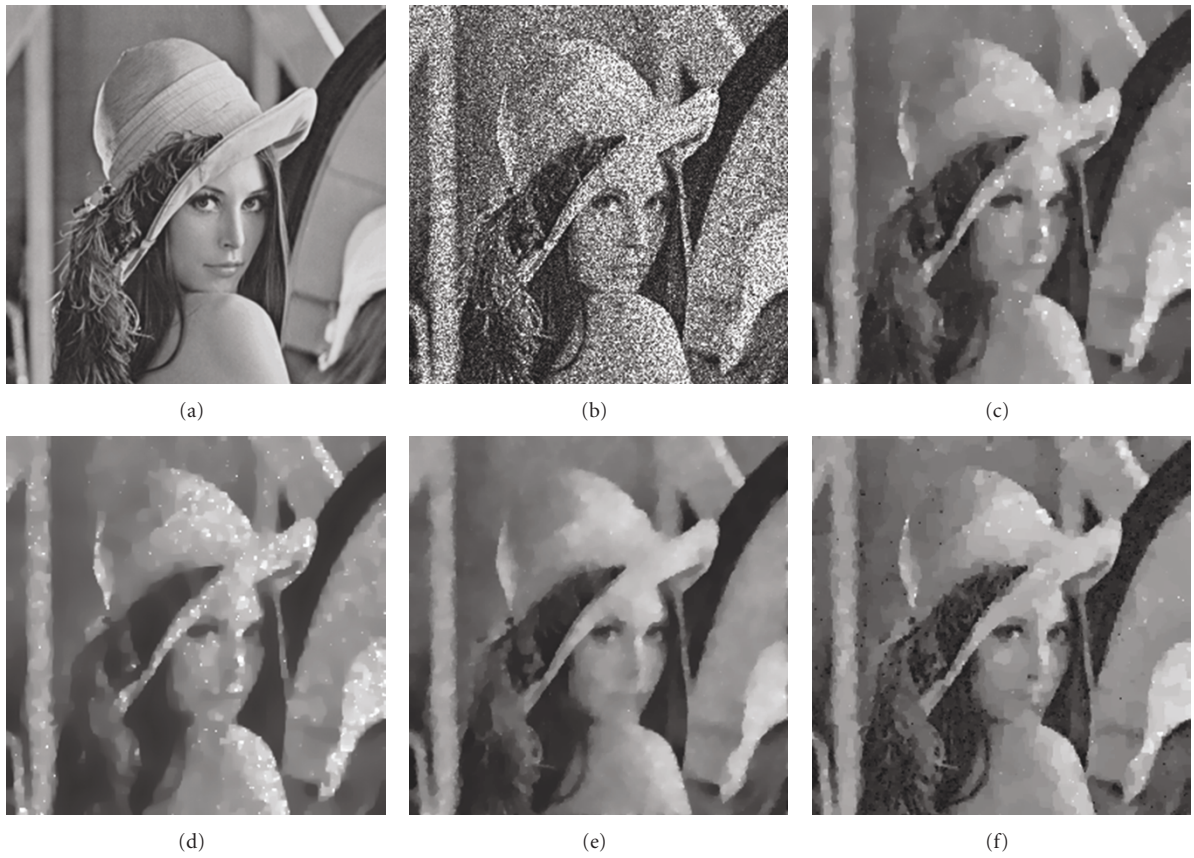

FIGURE 2: The original, noisy, and restored "Lena" images: (a) noiseless image; (b) noisy image with $L = 5$; denoised images by (c) RLO method; (d) AA method; (e) HMW method ($\alpha_1 = 19, \alpha_2 = 0.0160$); (f) the proposed method ($\alpha_1 = 0.004, \alpha_2 = 0.007$).

Applying the above lemma to our restoration functional, the formal Euler-Lagrange equation for any solution of problem (13) is as follows

$$-\frac{\alpha_1 u + \alpha_2}{u}\operatorname{div}\left(\frac{\nabla u}{\sqrt{|\nabla u|^2+\varepsilon}}\right) + \frac{u-f}{u^2} = 0 \quad \text{in } \Omega,$$
$$\frac{\partial u}{\partial \vec{n}} = 0 \quad \text{on } \partial\Omega. \tag{22}$$

Since $u > 0$, then the Euler-Lagrange equation (22) of minimizing can be rewritten equivalently as

$$-\operatorname{div}\left(\frac{\nabla u}{\sqrt{|\nabla u|^2+\varepsilon}}\right) + \frac{u-f}{u(\alpha_1 u + \alpha_2)} = 0 \quad \text{in } \Omega,$$
$$\frac{\partial u}{\partial \vec{n}} = 0 \quad \text{on } \partial\Omega. \tag{23}$$

Define $\widetilde{\lambda} = \widetilde{\lambda}(u) = 1/(u(\alpha_1 u + \alpha_2))$. Then (23) can be rewritten as

$$\nabla E(u) := -\operatorname{div}\left(\frac{\nabla u}{\sqrt{|\nabla u|^2+\varepsilon}}\right) + \widetilde{\lambda}(u-f) = 0 \quad \text{in } \Omega, \tag{24}$$

with the Neumann adiabatic condition along the boundary of the image domain. It is formally identical to the classical TV denoising equation [6, 29], except that the fitting constant λ now depends on u. Notice that $\widetilde{\lambda} > 0$ since $u > 0$.

Equations: (24) can be expressed in operator notation

$$L(u)u = \widetilde{\lambda}(u)f, \tag{25}$$

where $L(u)$ is the linear diffusion operator whose action on a function v is given by

$$L(u)v = -\operatorname{div}\left(\frac{\nabla v}{\sqrt{|\nabla u|^2+\varepsilon}}\right) + \widetilde{\lambda}(u)v. \tag{26}$$

The fixed point iteration is then

$$L\left(u^{(n)}\right)u^{(n+1)} = \widetilde{\lambda}\left(u^{(n)}\right)f, \ n = 0, 1, \ldots. \tag{27}$$

Finite difference method is used commonly for discretization of partial differential equation (PDE). Equations (25) can be approximately computed by the

(a) (b) (c)

(d) (e) (f)

Figure 3: The original, noisy, and restored "Cameraman" images: (a) noiseless image; (b) noisy image with $L = 13$; denoised images by (c) RLO method; (d) AA method; (e) HMW method ($\alpha_1 = 19, \alpha_2 = 0.0095$); (f) the proposed method ($\alpha_1 = 0.002, \alpha_2 = 0.0005$).

first-order accurate finite difference schemes described as follows [6]:

$$
\begin{aligned}
D_x^{\pm}\left(u_{i,j}\right) &= \pm\left[u_{i\pm1,j} - u_{i,j}\right],\\
D_y^{\pm}\left(u_{i,j}\right) &= \pm\left[u_{i,j\pm1} - u_{i,j}\right],\\
\left|D_x(u_{i,j})\right|_{\varepsilon} &= \sqrt{\left(D_x^{+}\left(u_{i,j}\right)\right)^2 + \left(m\left[D_y^{+}\left(u_{i,j}\right), D_y^{-}\left(u_{i,j}\right)\right]\right)^2 + \varepsilon},\\
\left|D_y(u_{i,j})\right|_{\varepsilon} &= \sqrt{\left(D_y^{+}\left(u_{i,j}\right)\right)^2 + \left(m\left[D_x^{+}\left(u_{i,j}\right), D_x^{-}\left(u_{i,j}\right)\right]\right)^2 + \varepsilon},
\end{aligned}
\tag{28}
$$

where $m[a,b] = (\operatorname{sign}(a) + \operatorname{sign}(b))/2 \cdot \min(|a|,|b|)$. Here, we denote the space step size by $h = 1$. These schemes yield approximate form of (26):

$$
L(u)v \approx \left(D_x^{-}\left(\frac{D_x^{+}v}{|D_x u|_{\varepsilon}}\right) + D_y^{-}\left(\frac{D_y^{+}v}{\left|D_y u\right|_{\varepsilon}}\right)\right) + \widetilde{\lambda}(u)v,
\tag{29}
$$

and matrix operators L (cf. (25)) which are symmetric and positive definite and sparse. In our computational experiments, ε is set to be 10^{-4}.

What follows is a generic algorithm for the minimization of $E(u)$ in (13). The superscript (n) denotes iteration count. ξ_1, ξ_2 are user-defined tolerance, $n_{\max}$ is an iteration limit, and $\|\cdot\|$ denotes the l^2 norm.

Input: $\varepsilon, \alpha_1, \alpha_2, \xi_1, \xi_2, n_{\max}$.

Initialization: $u^{(0)} = f, n = 0$.

(1) Compute a descent direction $d^{(n)}$ for E at $u^{(n)}$.

(2) $u^{(n+1)} = u^{(n)} + d^{(n)}$.

(3) Check stopping criteria (see [29]): $\|u^{(n+1)} - u^{(n)}\| \le \xi_1$ or $\|\nabla E(u^{(n+1)})\| \le \xi_2$ or $n \ge n_{\max}$.

In step 1, we set $d^{(n)} = u^{(n+1)} - u^{(n)}$ and yield

$$
\begin{aligned}
d^{(n)} &= -L\left(u^{(n)}\right)^{-1}\left(L\left(u^{(n)}\right)u^{(n)} - \widetilde{\lambda}\left(u^{(n)}\right)f\right)\\
&= -L\left(u^{(n)}\right)^{-1}\nabla E\left(u^{(n)}\right).
\end{aligned}
\tag{30}
$$

Equation (30) follows from (27) and (24), respectively. The conjugate gradient method applied to solve the above linear diffusion equations to get the $d^{(n)}$ and the stopping criterion of the inner conjugate gradient iteration is that the residual should be less than 10^{-4}. In our computational experiments, we set $\xi_1 = \xi_2 = 10^{-4}$, and $n_{\max} = 500$.

3.2. Parameters Choice. We remark that there are two regularization parameters α_1 and α_2 in the proposed algorithm,

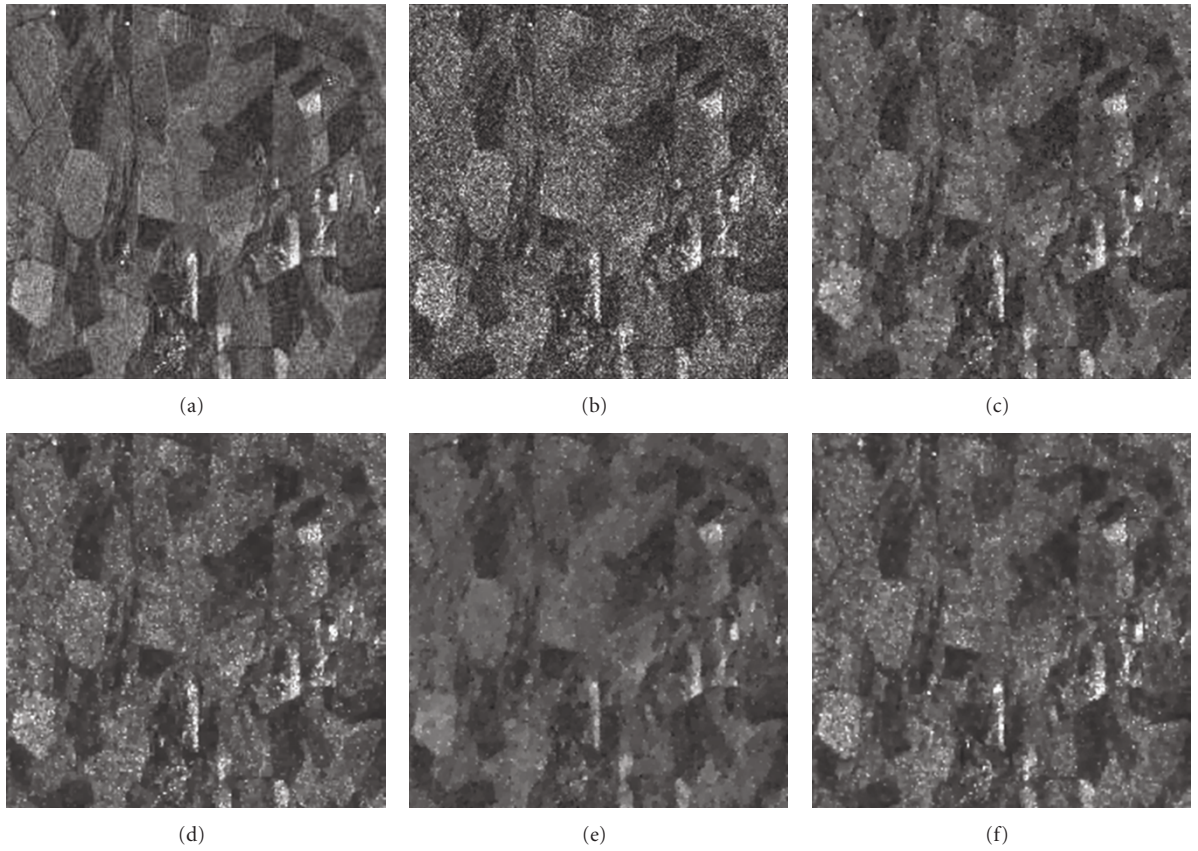

Figure 4: The original, noisy, and restored SAR images: (a) noiseless image; (b) noisy image with $L = 10$; denoised images by (c) RLO method; (d) AA method; (e) HMW method ($\alpha_1 = 19, \alpha_2 = 0.0050$); (f) the proposed method ($\alpha_1 = 0.005, \alpha_2 = 0.45$).

which controls the tradeoff between the image fidelity term and the regularization term. When $\alpha_2 = 0$, we note that our model (13) is the AA-model [18] as follows:

$$\min_u \alpha_1 \mathrm{TV}_\varepsilon(u) + \int_\Omega \left(\log u + \frac{f}{u}\right) \mathrm{d}x. \tag{31}$$

Borrowing the idea of [6], we dynamically compute the value of α_1 according to the variance of the recovered noise which matches that of our prior knowledge. The Gamma-distributed noise has the mean and variance as follows:

$$\int_\Omega f/u \ \mathrm{d}x = 1, \qquad \int_\Omega (f/u - 1)^2 \mathrm{d}x = \sigma^2. \tag{32}$$

The solution procedure uses a parabolic equation with time as an evolution parameter. This means that we solve

$$\begin{aligned} \frac{\partial u}{\partial t} &= \mathrm{div}\left(\frac{\nabla u}{\sqrt{|\nabla u|^2 + \varepsilon}}\right) + \alpha_3 \frac{f-u}{u^2}, \\ \frac{\partial u}{\partial \vec{n}}\bigg|_{\partial\Omega} &= 0, \end{aligned} \tag{33}$$

for $t > 0$. We merely multiply the first equation of (33) by $f - u$ and integrate by parts over Ω. If steady state has been reached, the left side of the first equation of (33) vanishes, and then we have

$$\alpha_1 = \frac{\sigma^2}{\int_\Omega \nabla u / \left(\sqrt{|\nabla u|^2 + \varepsilon}\right) \cdot \nabla (f-u) \ \mathrm{d}x}. \tag{34}$$

Then, we determine the best value of α_2 from their tested values such that the peak signal-to-noise ratio (PSNR, see definition here in after) of the restored image is the maximal.

3.3. Other Methods. We have compared our results with some other variational multiplicative denoising methods.

RLO Method. The solution of RLO-model [17] is obtained by using the following gradient projection iterative scheme [17] (the subscripts i, j are omitted):

$$\begin{aligned} u^{(n+1)} = u^{(n)} + \Delta t \Bigg[& \left(D_x^- \left(\frac{D_x^+ u^{(n)}}{\left| D_x u^{(n)} \right|_\varepsilon} \right) + D_y^- \left(\frac{D_y^+ u^{(n)}}{\left| D_y u^{(n)} \right|_\varepsilon} \right) \right) \\ & + \lambda \frac{f^2}{\left(u^{(n)} + \varepsilon\right)^3} + \mu \frac{f}{\left(u^{(n)} + \varepsilon\right)^2} \Bigg]. \end{aligned} \tag{35}$$

In our experiments, ε and time step size Δt are set to be 10^{-4} and 0.2, respectively. The two Lagrange multipliers λ

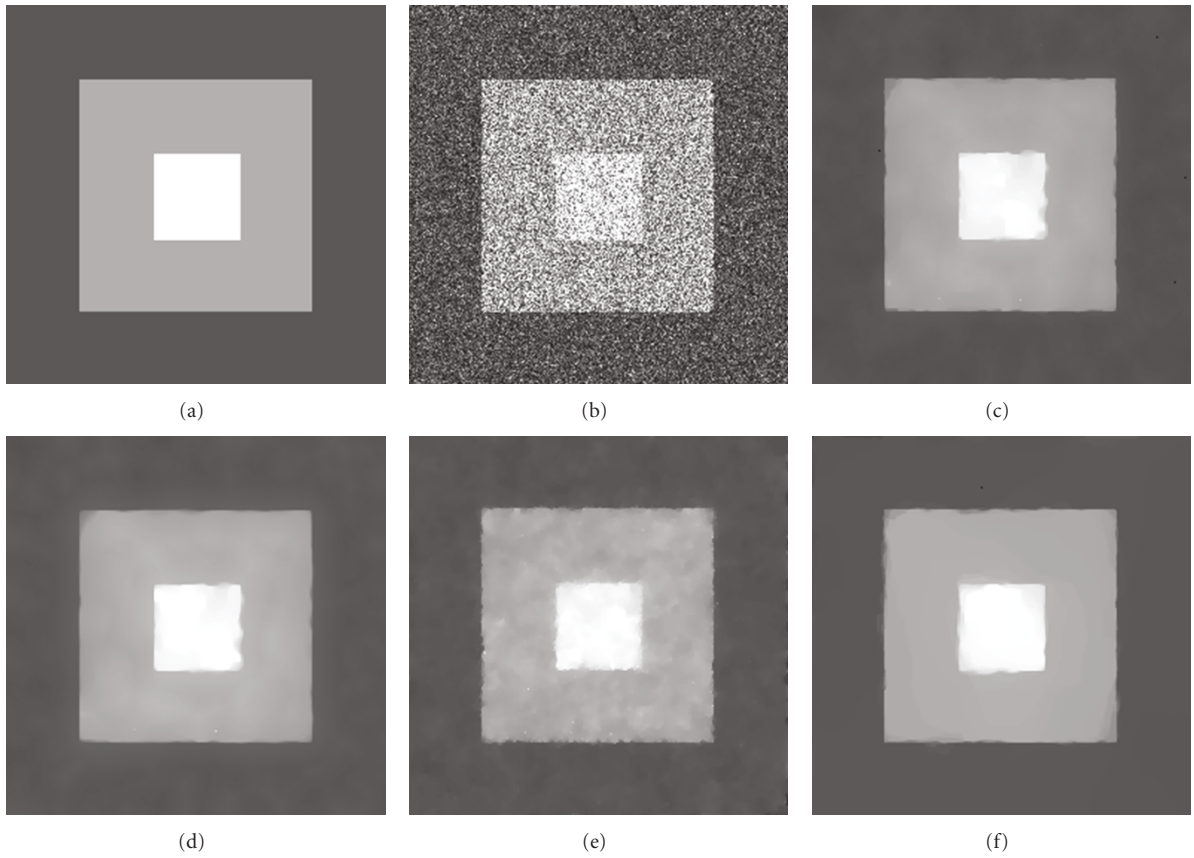

FIGURE 5: The original, noisy, and restored "SynImag1" images: (a) noiseless image; (b) noisy image with $L = 5$; denoised images by (c) RLO method; (d) AA method; (e) HMW method ($\alpha_1 = 19, \alpha_2 = 0.0150$); (f) the proposed method ($\alpha_1 = 0.01, \alpha_2 = 0.0095$).

and μ are dynamically updated to satisfy the constraints (as explained in [17]).

AA Method. The solution of AA-model [18] is obtained by using the gradient projection method:

$$u^{(n+1)} = u^{(n)} + \Delta t \left[\lambda \left(D_x^- \left(\frac{D_x^+ u^{(n)}}{\left| D_x u^{(n)} \right|_\varepsilon} \right) + D_y^- \left(\frac{D_y^+ u^{(n)}}{\left| D_y u^{(n)} \right|_\varepsilon} \right) \right) + \frac{f - u^{(n)}}{\left(u^{(n)} + \varepsilon \right)^2} \right]. \tag{36}$$

In our experiments, $\varepsilon, \Delta t$ take the same value in the RLO method. The regularization parameter λ is dynamically updated according to (34).

HMW Method. The solution of HMW-model [20] (we note that HMW-model is equivalent to SO-model as $\alpha_1 \to \infty$.)

$$\min_{z,w} \left\{ \sum_{i=1}^{N^2} \left([z]_i + [f]_i e^{-[z]_i} \right) + \alpha_1 \| z - w \|_2^2 + \alpha_2 \mathrm{TV}(w) \right\} \tag{37}$$

is obtained by using the following alternating minimization algorithm:

$$z^{(n)} = \arg\min_z \sum_{i=1}^{N^2} \left([z]_i + [f]_i e^{-[z]_i} \right) + \alpha_1 \left\| z - w^{(n-1)} \right\|_2^2,$$
$$w^{(n)} = \arg\min_w \left\{ \alpha_1 \left\| z^{(n)} - w \right\|_2^2 + \mathrm{TV}(w) \right\}. \tag{38}$$

The corresponding nonlinear Euler-Lagrange equation of z-subproblem of (3.12)

$$1 - [f]_i e^{-[z]_i} + 2\alpha_1 \left([z]_i - \left[w^{(n-1)} \right]_i \right) = 0, \quad i = 1, 2, \ldots, N^2, \tag{39}$$

was solved by using the Newton method. The Chambolle projection algorithm was employed in the denoising w-subproblem of (3.12) [20]. Then the restored image is computed by $\exp(w)$. Here, the rule to determine the two regularization parameters α_1, α_2 and the stopping criterion of the HMW method are chosen as suggested in [20].

In our computational experiments, we use the initial guess $u^{(0)} = f$ in RLO and AA method and $w^{(0)} = \log f$

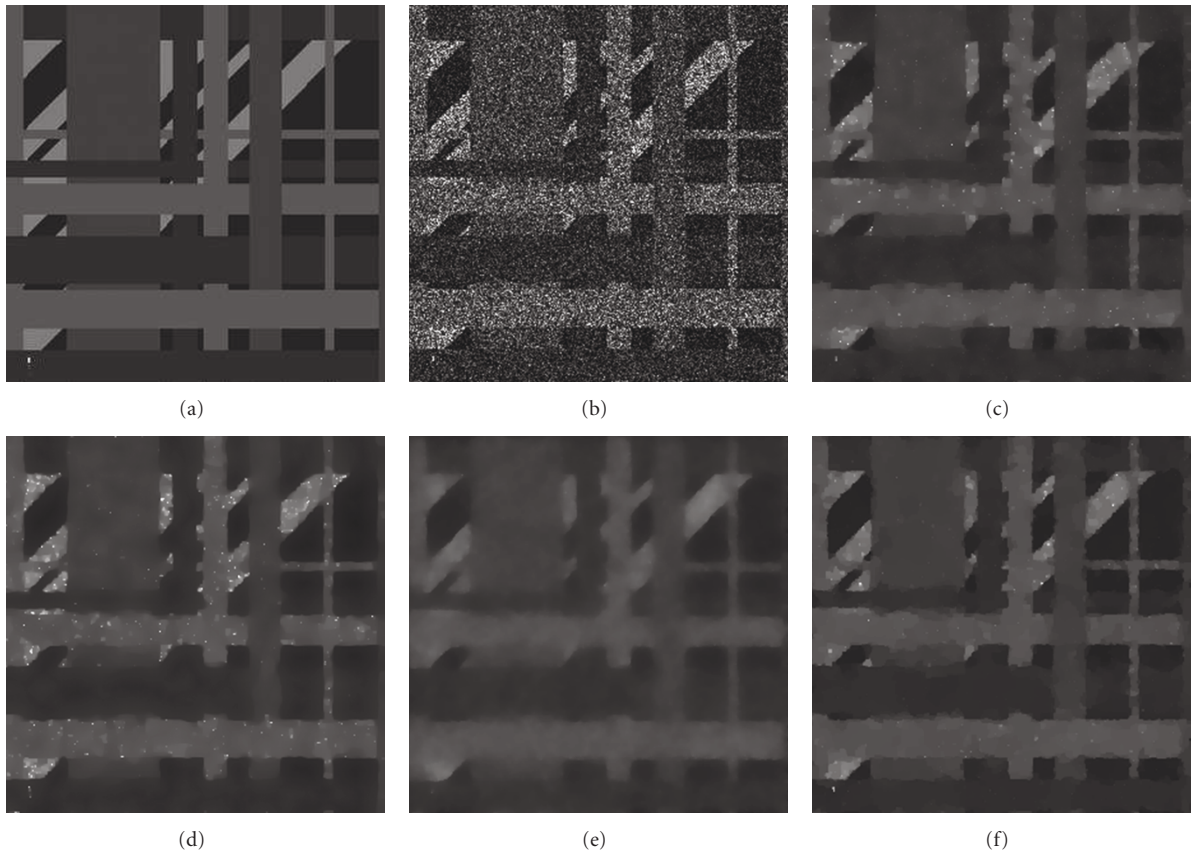

Figure 6: The original, noisy, and restored " SynImag2" images: (a) noiseless image; (b) noisy image with $L = 2$; denoised images by (c) RLO method; (d) AA method; (e) HMW method ($\alpha_1 = 19, \alpha_2 = 0.0400$); (f) the proposed method ($\alpha_1 = 0.005, \alpha_2 = 0.45$).

in HMW method. RLO and AA algorithms are terminated once they reached maximal PSNR.

3.4. Denoising of Color Images. In this subsection, we extend our approach to solve the multichannel version of (13). The general framework of the variational approach for color images processing based on the linear RGB color models can be classified into two categories—the channel-by-channel approach and the vectorial approach. Compared with the first approach, the second approach can exploit the spatial correlation and the spectral correlation in processing color images. So the vectorial approach has already been used in most of the literature for RGB images, such as the work of [31–33] solved multichannel total variation (MTV) regularization reconstruction problem. Considering that our multiplicative denoising variational model includes the Weberized TV regularizer, we choose the channel-by-channel approach in this paper for color image multiplicative noise removal due to its simplicity and robustness.

Recently, Zhang et al. [5] proposed an additive denoising scheme by using principal component analysis (PCA) with local pixel grouping (LPG). We refer to this method as LPG-PCA method. For a better preservation of image local structures, a pixel and its nearest neighbors are modeled as a vector variable, whose training samples are selected from the local window by using block matching-based LPG. The LPG-PCA denoising procedure is iterated one more time to further improve the denoising performance, and the noise level is adaptively adjusted in the second stage.

In our experiments, we only compare the denoising results of the noisy color images obtained by our approach with those obtained by the LPG-PCA method. We do it for the following two reasons: first, the LPG-PCA method using the channel-by-channel approach has been extended to solve the color image denoising problem; second, the multiplicative noise can be converted into additive noise by logarithmic transformation. In the LPG-PCA method, we make the size of the variable block and training block 2 and 20, respectively. We use $\log f$ as the initial guess. Then, the restored image is computed by exponential transform.

3.5. Results. The six test images (size: 256×256) used in the experiments, including five grey level images and one color image, are shown in Figures 1(a)–6(a) and Figures 9(a)–10(a), respectively. In our tests, each pixel of an original image is degraded by a noise which follows a Gamma distribution with density function in (3) and v is specified to have mean 1 and standard deviation $1/\sqrt{L}$. The noise level is controlled by the value of L in the experiments. The noisy images with different levels ($L = 33, 13, 10, 5, 2$) are shown in

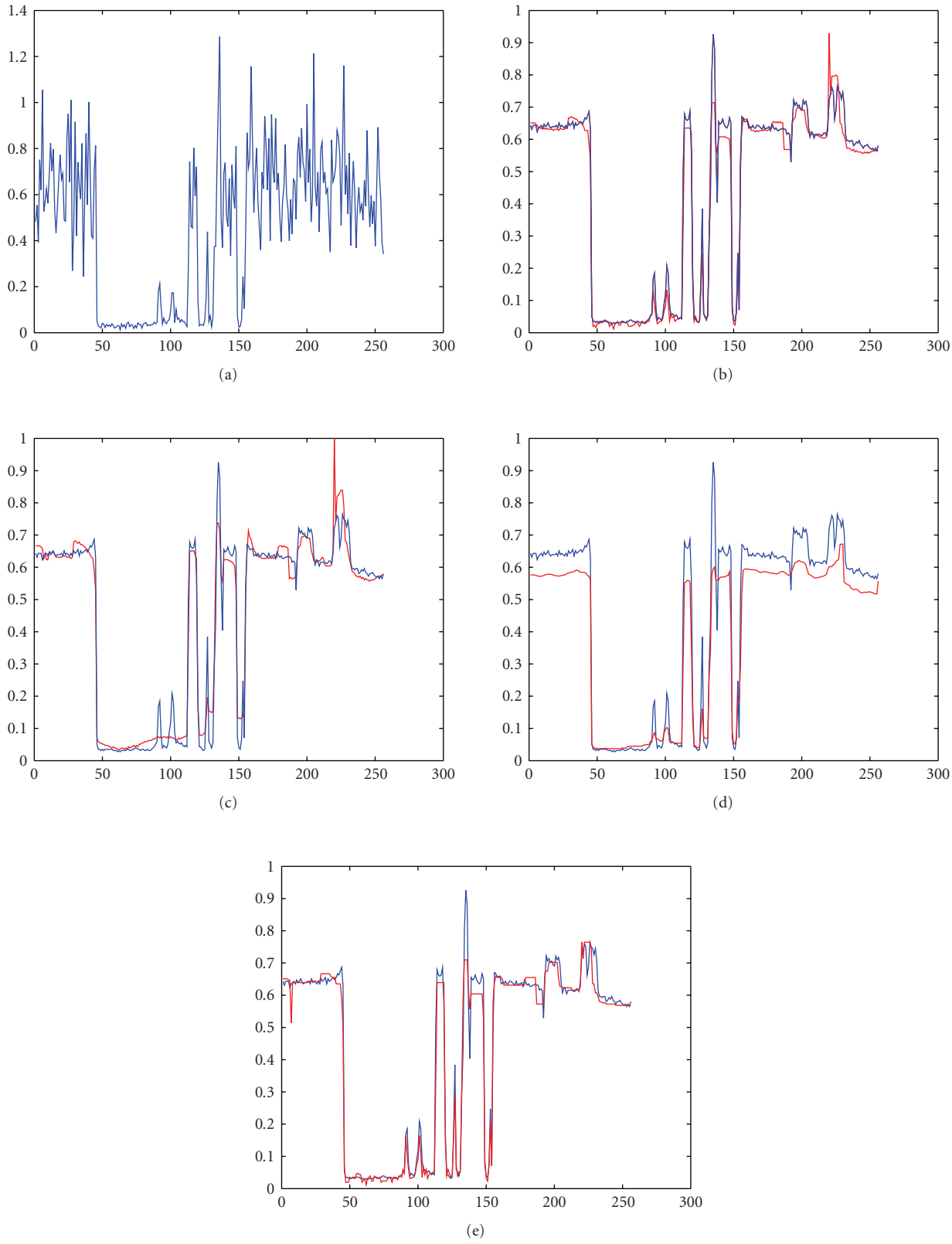

Figure 7: The 135th line of the original, noisy, and restored images of the "Cameraman" image. (a) The noisy slice; the slice restored by (b) the RLO method; (c) the AA method; (d) the HMW method; (e) the proposed method. Here the blue line is the original image, and the red line is the restored image.

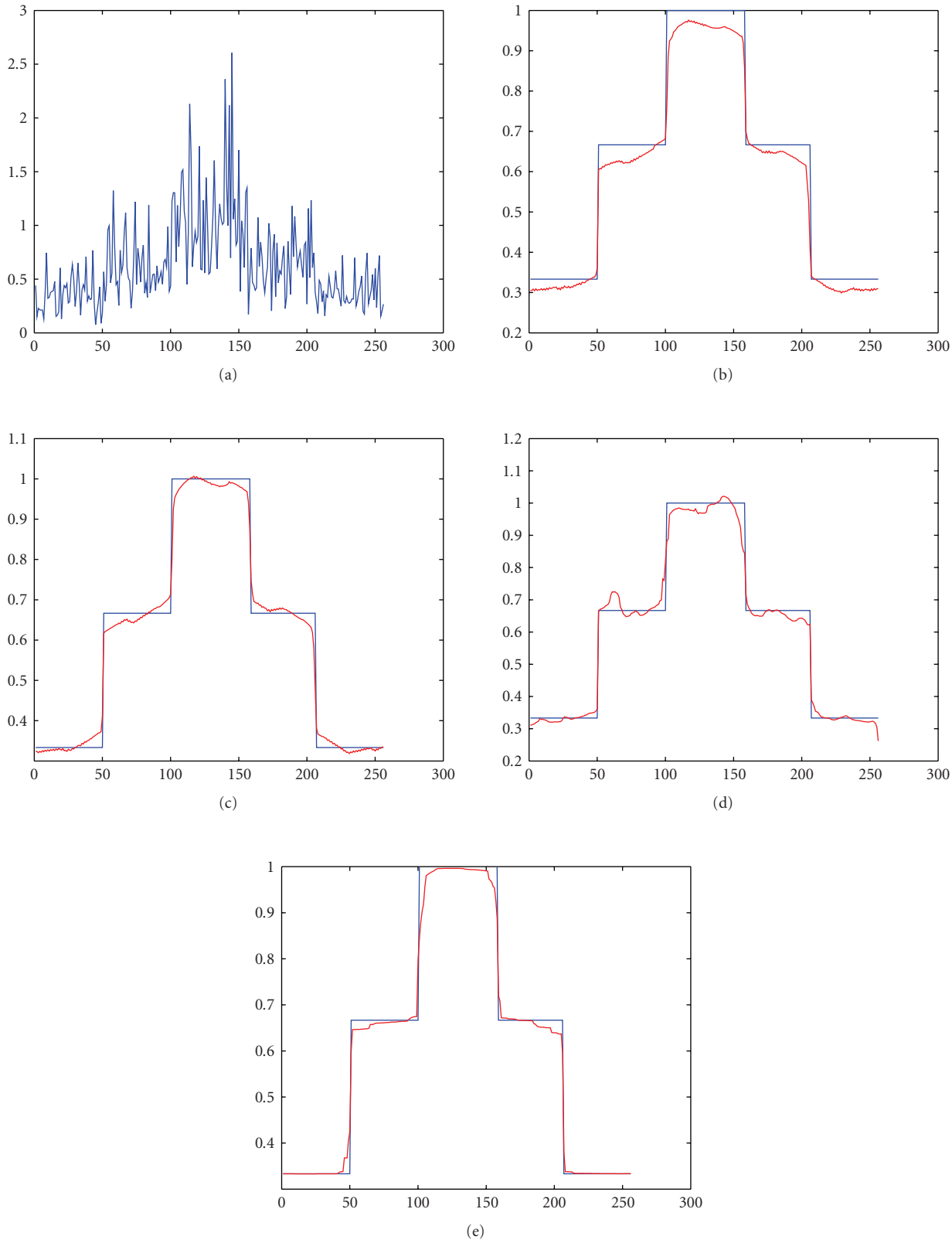

Figure 8: The 128th line of the original, noisy, and restored images of the "SynImag1" image. (a) The noisy slice; the slice restored by (b) the RLO method; (c) the AA method; (d) the HMW method; (e) the proposed method. Here the blue line is the original image, and the red line is the restored image.

(a) (b)

(c) (d)

Figure 9: The original, noisy, and restored color "Lena" images: (a) noiseless image; (b) noisy image with $L = 33$; denoised images by (c) LPG-PCA method; (d) the proposed method ($\alpha_1 = 0.001, \alpha_2 = 0.01$).

Figures 1(b)–6(b) and Figures 9(b)–10(b), respectively. We display the denoising results obtained by our approach as well as by the RLO, AA, HMW, and LPG-PCA methods.

We measure the quality of restoration by the peak signal-to-noise ratio (PSNR), the improved signal-to-noise ratio (ISNR), and the relative error (ReErr) of the restored image, defined by

$$\begin{aligned} \text{PSNR} &= 10\log_{10}\left\{\frac{M\times N\max\{u\}^2}{\|u^*-u\|^2}\right\},\\ \text{ISNR} &= 10\log_{10}\left\{\frac{\|f-u\|^2}{\|u^*-u\|^2}\right\},\\ \text{ReErr} &= \frac{\|u^*-u\|^2}{\|u\|^2}, \end{aligned} \tag{40}$$

where u, u^*, f, and $M \times N$ are the original, the restored, the observed image, and the size of the image, respectively.

Figures 1–6 show the denoising results of the six noisy gray level images by different methods. The subfigures (c–f) are the denoised images by the different methods. In these experiments, it is clear that the restoration results obtained by the proposed method are visually better than those by the HMW, AA, and RLO methods, especially when the noise variance is large, that is, when L is small. Although the most denoised images by the HMW method have better visual quality, we note that some details, such as camera and buildings in Figure 3(e) , become hazy. Such hazy details make the reconstructed image visually unpleased in some areas. Next we check the homogeneity of regions of interest in the image and analyze the loss (or the preservation) of contrast. In Figures 7 and 8, we show several lines of the original, noisy, and restored images. It is clear from the figures that the lines restored by the proposed method are better than those restored by the other three methods.

Table 1 lists the PSNR, ISNR, and ReErr results by different methods on the six noisy gray level images. From Table 1, we can see that the PSNRs and ISNRs of the images restored by using our method are more than those restored by using the other three methods, and ReErrs are less than the other four methods, except for the denoising results of Figure 4(b) obtained by the HMW method. In addition to the quality of the restored images, we also find that the proposed algorithm is efficient. Table 2 shows the number of iterations and the computational times required by the different algorithms. From Table 2, we see that the RLO algorithm takes more time than the other three methods. The spending time of our algorithm is in a middle position in comparison with the other three methods.

We now compare the LPG-PCA method with the proposed method on denoising the noisy color images.

(a) (b)

(c) (d)

Figure 10: The original, noisy, and restored color "Lena" images: (a) noiseless image; (b) noisy image with $L = 10$; denoised images by (b) LPG-PCA method; (c) the proposed method ($\alpha_1 = 0.003, \alpha_2 = 0.0001$).

Table 1: The PSNR (dB), ISNR (dB), and ReErr of the restored images using four methods.

Experiments	RLO method			AA method			HMW method			Our method		
	PSNR	ISNR	ReErr	PSNR	ISNR	ReErr	PSNR	ISNR	ReErr	PSNR	ISNR	ReErr
Figure 1(b)	27.646	7.580	0.0053	27.016	6.950	0.0061	27.944	7.629	0.0052	28.418	8.383	0.0044
Figure 2(b)	23.143	11.291	0.0150	22.554	10.702	0.0171	23.247	11.135	0.0154	23.620	11.702	0.0134
Figure 3(b)	25.736	9.094	0.0095	24.984	8.341	0.0113	25.513	8.865	0.0099	26.436	9.793	0.0081
Figure 4(b)	22.597	3.575	0.0441	22.369	3.374	0.0465	24.935	6.391	0.0231	22.993	3.930	0.0402
Figure 5(b)	29.713	16.978	0.0041	31.862	19.128	0.0025	30.690	17.885	0.0032	33.166	20.381	0.0018
Figure 6(b)	25.841	11.416	0.0361	25.717	11.292	0.0371	25.523	11.807	0.0331	26.951	12.489	0.0279

Table 2: The number of iterations (It no.), and computational times of four methods.

Experiments	RLO method		AA method		HMW method		Our method	
	It no.	CPU time (s)	It no.	CPU time (s)	It no.	CPU time (s)	ItNo.	CPU time (s)
Figure 1(b)	113	50.28	77	10.28	111	34.28	18	24.75
Figure 2(b)	344	153.38	272	36.63	155	46.84	79	109.48
Figure 3(b)	190	84.39	148	19.98	131	39.77	29	40.72
Figure 4(b)	78	23.89	49	3.63	174	31.94	5	3.95
Figure 5(b)	591	261.22	575	77.89	145	45.39	119	166.72
Figure 6(b)	251	152.92	246	42.78	188	84.63	53	100.03

Table 3: The PSNR (dB), ISNR (dB), ReErr, number of iterations (It no.) and computational times of the restored images using two methods.

	LPG-PCA method				Our method				
Experiments	PSNR	ISNR	ReErr	CPU time (s)	PSNR	ISNR	ReErr	ItNo.	CPU time (s)
Figure 9(b)	29.821	6.990	0.0061	1832	29.935	7.242	0.0057	17	79.31
Figure 10(b)	25.753	8.115	0.0155	1843	27.152	9.614	0.0109	27	129.53

Figures 9–10 show the denoising results by the two methods. Table 3 lists the PSNR, ISNR, and ReErr results, the number of iterations, and the computational times of the two algorithm. We see that although LPG-PCA method has the lower PSNR and ISNR measures and higher ReErrs than our method, their denoised images have better visual quality. The LPG-PCA method well preserves the image edges without introducing staircase effect. However, staircase effect is an innate defect of the TV regularization method. From Table 3, we also see that the LPG-PCA method consumes much time than our method to obtain comparable good images.

4. Conclusion

In this paper, we have studied a new nonconvex variational model for multiplicative noise removal under MAP framework. Then we prove the existence and uniqueness of a minimizer for the new model. Moreover, we develop an iterative algorithm based on the linearization technique for the associated nonlinear Euler-Lagrange equation and we demonstrate the good performance of the model on some numerical results. In the future, we will focus on resolving the two remaining problems. First, we will prove the uniqueness issue of the proposed model using the $\int_\Omega |Du|$ instead of $\int_\Omega |\nabla u| dx$ in BV. Second, we will give the convergence proof of our algorithm.

Appendix

Proof of Theorems 1 and 2

To prove the existence Theorem 1, we first give a Maximum Principle type result for the energy form (13).

Lemma A.3. *Suppose that $f \in L^\infty(\Omega)$ with $\inf_\Omega f > 0$; the solution $\hat{u}$ of the problem (13) has the following property:*

$$0 < \inf_\Omega f \le \hat{u} \le \sup_\Omega f. \tag{A.1}$$

Proof. The similar assertion appears in [18]; we detail the argument for completeness. Let $\alpha = \inf f$, and $\beta = \sup f$. We remark that $\log x + f/x$ is strictly increasing for $x > f$. Hence, we have that

$$\int_\Omega \left(\log(\inf(u,\beta)) + \frac{f}{\inf(u,\beta)}\right) dx \le \int_\Omega \left(\log u + \frac{f}{u}\right) dx. \tag{A.2}$$

Moreover, we have that (see [34, Lemma 1 in Section 4.3], [21, Lemma 1 in Section 3.2])

$$\mathrm{TV}(\inf(u,\beta)) \le \mathrm{TV}(u),\ \mathrm{TV}(\log(\inf(u,\beta))) \le \mathrm{TV}(\log u). \tag{A.3}$$

Therefore we deduce that

$$E(\inf(u,\beta)) \le E(u), \tag{A.4}$$

and the equality holds if and only if $u \le \beta$, a.e. Since $\hat{u}$ is a minimizer in $\Pi(\Omega)$, the equality must hold and thus $u \le \beta$, a.e. We get in the same way that

$$E(\sup(u,\alpha)) \le E(u), \tag{A.5}$$

and thus $\hat{u} \ge \alpha$. □

Based on aforementioned lemma, now we are ready to give the proof of Theorem 1.

Proof of Theorem 1. Without loss of generality, we assume that $\alpha_1 = \alpha_2 = 1$. Applying ideas in [24], let us denote that $\alpha = \inf f$, and $\beta = \sup f$. We note that the admissible space $\Pi(\Omega)$ is nonempty since $u \equiv \beta \in \Pi(\Omega)$. Let $\{u_n\} \subset \Pi(\Omega)$ be a minimizing sequence for problem (13). Thanks to Lemma 2, we can assume that $\alpha \le u_n \le \beta$. This implies that $\|u_n\|_{L^1(\Omega)}$ is bounded (Ω is bounded).

For a sequence $\{u_n\}$, we have $E(u_n) \le C$, where C is a constant. Since $\mathrm{TV}(\log u_n) < \infty$ and $\int_\Omega (\log u_n + f/u_n) dx$ reaches its minimum value $\int_\Omega (1 + \log f) dx$ when $u = f$, we get that u_n is bounded in $\mathrm{BV}(\Omega)$.

Thus, up to a subsequence, there exists u in $\mathrm{BV}(\Omega)$ such that $u_n \to u$ in $L^1(\Omega)$-strong. Furthermore, after a refinement of the subsequence if necessary, we can assume that

$$u_n(x) \longrightarrow u(x), \quad a.e.\ x \in \Omega. \tag{A.6}$$

Using the Lebesgue Dominated Convergence Theorem, then we have

$$\int_\Omega \left(\log u + \frac{f}{u}\right) dx = \lim_{n\to\infty} \int_\Omega \left(\log u_n + \frac{f}{u_n}\right) dx. \tag{A.7}$$

Next we prove that $J(u)$ is lower semicontinuity. Firstly, from the properties of the $BV(\Omega)$ [7], we have

$$\int_\Omega |Du| \le \liminf_{n\to\infty} \int_\Omega |Du_n|. \tag{A.8}$$

Secondly, the lower semicontinuity of Weberized TV can also be proved. Let us define $v_n = \log u_n$ and $v = \log u$; then

$$v_n(x) \to v(x), \quad a.e.\ x \in \Omega. \tag{A.9}$$

Let $p \in C_0^1(\Omega, R^2)$ be a vector-valued function such that $\| |p| \|_\infty \leq 1$. We have

$$v_n \nabla \cdot p \to v \nabla \cdot p, \quad \text{a.e. } x \in \Omega, \tag{A.10}$$

and also

$$|v_n \nabla \cdot p| \leq |\log \beta| \, |\nabla \cdot p| \, a.e. \tag{A.11}$$

Since p is compactly supported, the right side of the above inequality belongs to $L^1(\Omega)$. Therefore, again by the Lebesgue Dominated Convergence Theorem,

$$\int_\Omega v \nabla \cdot p \, dx = \lim_{n \to \infty} \int_\Omega v_n \nabla \cdot p \, dx \leq \liminf_{n \to \infty} \int_\Omega |Dv_n|. \tag{A.12}$$

Now take sup over p to get

$$\int_\Omega |Dv| \leq \liminf_{n \to \infty} \int_\Omega |Dv_n|. \tag{A.13}$$

Combining (A.1), (A.2), and (A.3), we have

$$E(u) \leq \liminf_{n \to \infty} E(u_n). \tag{A.14}$$

It is easy to see that $u \in \Pi(\Omega)$. Since u_n is a minimizing sequence, we therefore have shown that u is in fact a minimizer. □

Based on the theory of optimization, an objective function possesses a unique minimizer when it is strictly convex and coercive [35]. Since the negative log-likelihood and Weberized TV prior are not convex, as a result, the restoration energy $E(u)$ in (13) is not convex and uniqueness is no longer a direct product of convexity. We address the problem of the uniqueness of the solution of problem (13), which relies on the formal Euler-Lagrange equation of (13):

Proof of Theorem 2. Let us denote

$$F'(u; \alpha_1, \alpha_2) = \frac{u - f}{u(\alpha_1 u + \alpha_2)}. \tag{A.15}$$

Define a new reference energy $E_r(u)$ for the restoration energy $E(u)$ as follows:

$$E_r(u) = \int_\Omega \left(\sqrt{|\nabla u|^2 + \varepsilon} + F(u; \alpha_1, \alpha_2) \right) dx. \tag{A.16}$$

It is easy to derive that (23) is exactly the Euler-Lagrange equilibrium equation for $E_r(u)$. We have

$$F''(u; \alpha_1, \alpha_2) = \frac{-\alpha_1 u^2 + 2\alpha_1 f u + \alpha_2 f}{(\alpha_1 u^2 + \alpha_2 u)^2}. \tag{A.17}$$

We deduce that if (18) holds, then $F'' > 0$ and F is strictly convex. Now that the TV Radon measure is semiconvex, so the objective function $E_r(u)$ is globally strictly convex and possesses a uniqueminimizer. □

Acknowledgments

The authors thank the authors of [5, 20] for sharing their programs. Moreover, they would like to express their gratitude to the anonymous referees and editor for making helpful and constructive suggestions. This work was supported in part by the Natural Science Foundation of China under Grant nos. 60802039 and 60672074, by the National 863 High Technology Development Project under Grant no. 2007AA12Z142, by the Doctoral Foundation of Ministry of Education of China under Grant no. 200802880018, and by the Scientific Innovation project of Nanjing University of Science and Technology no. 2010ZDJH07.

References

[1] D. L. Donoho and M. Johnstone, "Adapting to unknown smoothness via wavelet shrink-age," *Journal of the American Statistical Association*, vol. 90, no. 432, pp. 1200–1224, 1995.

[2] P. Bao and L. Zhang, "Noise reduction for magnetic resonance images via adaptive multiscale products thresholding," *IEEE Transactions on Medical Imaging*, vol. 22, no. 9, pp. 1089–1099, 2003.

[3] S. Geman and D. Geman, "Stochastic relaxation, Gibbs distributions, and the Bayesian restoration of images," *IEEE Transactions on Pattern Analysis and Machine Intelligence*, vol. 6, no. 6, pp. 721–741, 1984.

[4] L. Zhang, R. Lukac, X. Wu, and D. Zhang, "PCA-based spatially adaptive denoising of CFA images for single-sensor digital cameras," *IEEE Transactions on Image Processing*, vol. 18, no. 4, pp. 797–812, 2009.

[5] L. Zhang, W. Dong, D. Zhang, and G. Shi, "Two-stage image denoising by principal component analysis with local pixel grouping," *Pattern Recognition*, vol. 43, no. 4, pp. 1531–1549, 2010.

[6] L. I. Rudin, S. Osher, and E. Fatemi, "Nonlinear total variation based noise removal algorithms," *Physica D*, vol. 60, no. 1–4, pp. 259–268, 1992.

[7] G. Aubert and P. Kornprobst, *Mathematical Problems in Image Processing*, vol. 147 of *Applied Mathematical Sciences*, Springer, Berlin, Germany, 2002.

[8] A. Buades, B. Coll, and J. M. Morel, "A review of image denoising algorithms, with a new one," *Multiscale Modeling and Simulation*, vol. 4, no. 2, pp. 490–530, 2005.

[9] H. Lewis, *Principle and Applications of Imaging Radar*, vol. 2 of *Manual of Remote Sensing*, John Wiley & Sons, New York, NY, USA, 3rd edition, 1998.

[10] J. S. Lee, "Digital image enhancement and noise filtering by use of local statistics," *IEEE Transactions on Pattern Analysis and Machine Intelligence*, vol. 2, no. 2, pp. 165–168, 1980.

[11] D. T. Kuan, A. A. Sawchuk, T. C. Strand, and P. Chavel, "Adaptive noise smoothing filter for images with signal-dependent noise," *IEEE Transactions on Pattern Analysis and Machine Intelligence*, vol. 7, no. 2, pp. 165–177, 1985.

[12] Y. Yu and S. T. Acton, "Speckle reducing anisotropic diffusion," *IEEE Transactions on Image Processing*, vol. 11, no. 11, pp. 1260–1270, 2002.

[13] S. Aja-Fernández and C. Alberola-López, "On the estimation of the coefficient of variation for anisotropic diffusion speckle filtering," *IEEE Transactions on Image Processing*, vol. 15, no. 9, pp. 2694–2701, 2006.

[14] K. Krissian, C.-F. Westin, R. Kikinis, and K. G. Vosburgh, "Oriented speckle reducing anisotropic diffusion," *IEEE Transactions on Image Processing*, vol. 16, no. 5, pp. 1412–1424, 2007.

[15] G. Liu, X. Zeng, F. Tian, Z. Li, and K. Chaibou, "Speckle reduction by adaptive window anisotropic diffusion," *Signal Processing*, vol. 89, no. 11, pp. 2233–2243, 2009.

[16] C. A. Deledalle, L. Denis, and F. Tupin, "Iterative weighted maximum likelihood denois-ing with probabilistic patch-based weights," *IEEE Transactions on Image Processing*, vol. 18, no. 12, pp. 2661–2672, 2009.

[17] L. I. Rudin, P. L. Lions, and S. Osher, "Multiplicative denoising and deblurring: theory andalgorithms," in *Geometric Level Set Methods in Imaging, Vision, and Graphics*, S. Osher and N. Paragios, Eds., pp. 103–120, Springer, Berlin, Germany, 2003.

[18] G. Aubertt and J.-F. Aujol, "A variational approach to removing multiplicative noise," *SIAM Journal on Applied Mathematics*, vol. 68, no. 4, pp. 925–946, 2008.

[19] J. Shi and S. Osher, "A nonlinear inverse scale space method for a convex multiplicative noise model," *SIAM Journal on Imaging Sciences*, vol. 1, no. 3, pp. 294–321, 2008.

[20] Y. M. Huang, M. K. Ng, and Y. W. Wen, "A new total variation method for multiplicativenoise removal," *SIAM Journal on Imaging Sciences*, vol. 2, no. 1, pp. 22–40, 2009.

[21] D. J. Bioucas and M. Figueiredo, "Total variation restoration of speckled images using a split-Bregman algorithm," in *Proceedings of IEEE International Conference on Image Processing (ICIP '2009)*, Cairo, Egypt, 2009.

[22] G. Steidl and T. Teuber, "Removing multiplicative noise by douglas-rachford splitting methods," *Journal of Mathematical Imaging and Vision*, vol. 36, no. 2, pp. 168–184, 2010.

[23] S. Durand, J. Fadili, and M. Nikolova, "Multiplicative noise cleaning via a variational methodinvolving curvelet coe±cients," in *Scale Space and Variational Methods*, A. Lie, M. Lysaker, K. Morken, and X.-C. Tai, Eds., Springer, Voss, Norway, 2009.

[24] J. Shen, "On the foundations of vision modeling: I. Weber's law and Weberized TV restoration," *Physica D*, vol. 175, no. 3-4, pp. 241–251, 2003.

[25] J. Shen and Y.-M. Jung, "Weberized mumford-shah model with bose-einstein photon noise," *Applied Mathematics and Optimization*, vol. 53, no. 3, pp. 331–358, 2006.

[26] Z. Wei, Y. Fu, Z. Gao, and S. Cheng, "Visual compander in wavelet-based image coding," *IEEE Transactions on Consumer Electronics*, vol. 44, no. 4, pp. 1261–1266, 1998.

[27] Z. H. Wei, P. Qin, and Y. Q. Fu, "Perceptual digital watermark of images using wavelet transform," *IEEE Transactions on Consumer Electronics*, vol. 44, no. 4, pp. 1267–1272, 1998.

[28] E. H. Weber, "De pulsu, resorptione, audita et tactu," in *Annotationes anatomicae et physio-logicae*, Koehler, Leipzig, Germany, 1834.

[29] C. R. Vogel and M. E. Oman, "Iterative methods for total variation denoising," *SIAM Journal of Scientific Computing*, vol. 17, no. 1, pp. 227–238, 1996.

[30] T. F. Chan, S. Osher, and J. Shen, "The digital TV filter and nonlinear denoising," *IEEE Transactions on Image Processing*, vol. 10, no. 2, pp. 231–241, 2001.

[31] J. Yang, W. Yin, Y. Zhang, and Y. Wang, "A fast algorithm for edge-preserving variationalmultichannel image restoration," *SIAM Journal on Imaging Sciences*, vol. 2, no. 1, pp. 569–592, 2009.

[32] A. Brook, R. Kimmel, and N. A. Sochen, "Variational restoration and edge detection for color images," *Journal of Mathematical Imaging and Vision*, vol. 18, no. 3, pp. 247–268, 2003.

[33] T. Chan and J. Shen, "Variational restoration of nonflat image features: models and algorithms," *SIAM Journal on Applied Mathematics*, vol. 61, no. 4, pp. 1338–1361, 2000.

[34] S. Mallat, *A Wavelet Tour of Signal Processing*, Academic Press, New York, NY, USA, 1999.

[35] P. L. Combettes and V. R. Wajs, "Signal recovery by proximal forward-backward splitting," *Multiscale Modeling and Simulation*, vol. 4, no. 4, pp. 1168–1200, 2005.